Sustainable Cities and Society 56 (2020) 102075

Contents lists available at ScienceDirect

Sustainable Cities and Society

journal homepage: www.elsevier.com/locate/scs

Assessing impacts of climate change and human activities on the abnormal correlation between actual evaporation and atmospheric evaporation demands in southeastern China

Hua Bai[a,b,c], Xianghui Lu[b], Xiaoxiao Yang[d], Jianchu Huang[d], Xingmin Mu[a,c,*], Guangju Zhao[a,c], Faliang Gui[b], Chao Yue[a,c]

[a] Institute of Soil and Water Conservation, Chinese Academy of Sciences and Ministry of Water Resources, Yangling, Shaanxi 712100, China
[b] Jiangxi Key Laboratory of Hydrology-Water Resources and Water Environment, Nanchang Institute of Technology, Nanchang, Jiangxi 330099, China
[c] University of Chinese Academy of Sciences, Beijing 100049, China
[d] Jiangxi Provincial Bureau of Hydrology, Nanchang, Jiangxi 330002, China

ARTICLE INFO

Keywords:
Climate change
Afforestation
Penman equation
Budyko-type equation
Water-energy balance
Complementary relationship of evaporation

ABSTRACT

Generally, atmospheric evaporation demand (*AED*) shows a positive correlation with actual evaporation (*AE*) in the Yangtze River basin. In order to explore whether and why abnormal correlation exits in its five sub-basins, the temporal changes between *AED* and *AE* were compared, and then the impacts of climate change and human activities on abnormal correlations were assessed using the sensitivity method of Penman equation and the decomposition method of Budyko equation. The results indicated: (1) Pan evaporation and potential evaporation (indicators of *AED*) decreased at rates of up to -0.04 and -0.06 mm d^{-1} $decade^{-1}$, respectively. In contrast, the water budget-derived evaporation (an indicator of *AE*) increased at the rate of 0.09 mm d^{-1} $decade^{-1}$ in the Fuhe River basin and remained stable in other basins. Abnormal correlations (nonpositive correlations) were observed. (2) Decreasing net radiation and wind speed were major climate factors resulting in simultaneous temporal decreases in *AED* and *AE*. In contrast, afforestation was a major human factor leading to an increase in annual *AE* of 78 mm, but had no effect on *AED*. Afforestation was the primary driving force of the abnormal correlation. These results could provide water-energy guidance for urban climate change mitigation and flood/drought disaster management.

1. Introduction

The mechanism of the water-energy balance transformation is a basic, crucially investigated issue in urban hydrology in response to a changing environment that is mainly dominated by rapid urbanization, ecological restoration, and climate change (Remondi, Burlando, & Vollmer, 2016). Characterization of the controlling factors and their linkages with other environmental elements to form a full picture of the water-energy cycle has provided a more complete description of the response mechanisms involved (Brutsaert & Parlange, 1998; Yang et al., 2007). Evaporation is the controlling environmental factor because it connects the water and energy cycles (Milly, 1994; Wolock & McCabe, 1999; Yang et al., 2007). The correlation between atmospheric evaporation demand (*AED*) and actual evaporation (*AE*) quantifies the regional water-energy balance. The appearance of an abnormal correlation (AC) indicates the existence of a regional water-energy balance transformation. Identifying its driving force will be beneficial for understanding the response mechanism of how the water-energy balance transforms in response to a changing environment. Such an understanding can also specify the variation in the boundary conditions in order to predict urban water-energy processes (Ali, Shafiee, & Berglund, 2017), which can then be applied to address the urban heat island effect (Giridharan & Emmanuel, 2018; Roberge & Sushama, 2018), greenhouse gas emissions (Hardin et al., 2017), drought (Gober, Sampson, Quay, White, & Chow, 2016), and flood disasters (Nachshon, Netzer, & Livshitz, 2016) in a changing environment.

Water budget-derived evaporation (*WBDE*) using the surface water balance method is the proper basin-wide *AE* index, while potential evaporation (ET_p) and pan evaporation (E_{pan}) are the appropriate indicators of *AED*. Current observational and estimation methods of *AE*

* Corresponding author at: State Key Laboratory of Soil Erosion and Dryland Farming on the Loess Plateau, Northwest A&F University, 26 Xinong Road, Yangling, 712100, Shaanxi Province, China.
E-mail address: xmmu@ms.iswc.ac.cn (X. Mu).

https://doi.org/10.1016/j.scs.2020.102075
Received 30 January 2019; Received in revised form 2 September 2019; Accepted 26 January 2020
Available online 31 January 2020
2210-6707/ © 2020 Elsevier Ltd. All rights reserved.

mainly include the lysimeter, eddy covariance, Bowen ratio (Wang & Dickinson, 2012; World Meteorological Organization (WMO) (2014)), scintillometer, surface water balance, and atmospheric water balance methods (Wang & Dickinson, 2012). These methods have different spatial scales. Only the surface and atmospheric water balance methods are suitable for the basin scale (up to thousands of kilometres), while other methods are applicable for scales below hundreds of meters (DeBruin, 2009; Moene, Beyrich, & Hartogensis, 2009; Solignac et al., 2009; Wang & Dickinson, 2012). However, substantial errors have been found in estimates made by the atmospheric water balance method (Roads, 2003; Wang & Dickinson, 2012). Therefore, the surface water balance method is the appropriate method for directly obtaining *AE* at the basin scale. *AED* is estimated by reference evapotranspiration (ET_r) or ET_p and is measured by E_{pan}. But these two measures are intended for different applications. ET_r has been applied for irrigation scheduling using prescribed crop coefficients (Allen, Pereira, Raes, & Smith, 1998). In contrast, E_{pan} and ET_p are used for estimating open water evaporation (Fu, Liu, Chen, & Hong, 2004; Fu, Charles, & Yu, 2009; Penman, 1948), as well as for estimating basin-wide *AE* according to hypotheses regarding relationships with *AE* (Bouchet, 1963; Budyko, 1974; Penman, 1948; Sun, 2007; Yang, Sun, Liu, Cong, & Lei, 2006). Accordingly, E_{pan} and ET_p are the suitable indicators for estimating basin-wide *AE*.

The Bouchet's complementary hypothesis (BCH) and the Penman hypothesis (PH) are proposed to describe the correlation between *AE* and *AED* in arid and humid regions, respectively. Specifically, in arid and humid regions, also known as water-limited and energy-limited regions, evaporation is limited by available water and energy, respectively. An intermediate region is limited by both available water and energy. These regions are distinguished by different climatological aridity index (*CAI*) values, defined as the ratio of mean annual ET_p to precipitation (*P*). Water-limited and energy-limited regions are defined with $CAI \geq 1.35$ and $CAI \leq 0.76$, respectively, while an intermediate region is characterized by $0.76 < CAI < 1.35$ (McVicar, Roderick, Donohue, & Niel, 2012; Zhang et al., 2012). In energy-limited regions, *AED* is generally positively correlated with *AE* according to PH (Penman, 1948; Yang et al., 2006). In contrast, in water-limited regions, *AED* is negatively correlated with *AE* according to BCH (Bouchet, 1963; Zuo et al., 2016). In intermediate regions, the correlation between *AE* and *AED* tends to be explained by both PH and BCH. Even though PH and BCH appear as alternative hypotheses, they can be unified in the Budyko framework (Budyko, 1974; Sun, 2007).

Assessment of the temporal trends of *AED* and *AE* have been summarized to verify these hypotheses. Annual pan evaporation has steadily decreased since 1960 in most regions across the world, such as Russia, Siberia (Golubev et al., 2001; Peterson, Golubev, & Groisman, 1995), England and Scotland (Stanhill & Möller, 2008), Italy (Moonen, Ercoli, Mariotti, & Masoni, 2002), arid regions of China, eastern China, all of China (Liu, Xu, Henderson, & Gong, 2004; Shen, Liu, Liu, Zeng, & Tian, 2010; Xu, Pan, Gao, Fu, & Chiang, 2016; Yang & Yang, 2012), India (Chattopadhyay & Hulme, 1997), Australia, and New Zealand (Roderick & Farquhar, 2004; 2005). During the same period, annual ET_p has decreased in northwest and southeast China (Chen, Gao, Xu, Guo, & Ren, 2005; Thomas, 2000), all of China (Wang et al., 2017; Zhang et al., 2019), and India (Chattopadhyay & Hulme, 1997), but increased in Australia and New Zealand (Hobbins, Dai, Roderick, & Farquhar, 2008), south Florida (Abtew, Obeysekera, & Iricanin, 2010), North America (Hember, Coops, & Spittlehouse, 2017), northeast and southwest China (Chen et al., 2005; Thomas, 2000), and Romania (Croitoru, Piticar, Dragotă, & Burada, 2013). In contrast, the temporal trends of *WBDE* have been reported as both positive and negative (Ukkola & Prentice, 2013), and these trends are overwhelmingly influenced by *P*. Precipitation can explain 45–46 % of *AE* trends in energy-limited basins and 80–84 % in water-limited basins (Ukkola & Prentice, 2013).

By comparing the temporal trends of *AED* and *AE* in the studies mentioned above, the BCH and PH have been confirmed in water-limited and energy-limited regions, respectively. However, Bouchet's complementary relationship (BCR) between *AED* and *AE*, denoted by their negative correlation, has been observed in parts of typically energy-limited regions (Wang et al., 2011), especially in the regions covered with dense forest (Carmona, Poveda, Sivapalan, Vallejo-Bernal, & Bustamante, 2016; Lawrimore & Peterson, 2000) and urban areas (Nakamichi & Moroizumi, 2015). In these regions, the expected positive correlation between *AE* and *AED* for the entire energy-limited region was transformed into a negative relationship. Potential driving forces of this abnormal correlation (AC) were climate change or human activities (Arora, 2002). For instance, the aridification of parts of an energy-limited region could increase *CAI* more than the threshold *CAI* value of a water-limited region, thus leading to the AC (Zhang et al., 2012; McVicar, Roderick, Donohue, Niel et al., 2012). Human activities (*e.g.,* ecological restoration, rapid urbanization) could increase water and energy consumption (Hong et al., 2019; Wang, Feng, Zuo, & Rameezdeen, 2019) to alter the water-energy balance, and eventually change the positive correlation. Therefore, further investigations are needed to determine which variable is driving this abnormal correlation between *AE* and *AED*: climate change or human activities? This paper focuses on river basins in an energy-limited region of southeast China. These basins have experienced strong afforestation and urbanization in last 30 years compared with adjacent basins. The objective of this study was to identify the appearance of AC and to determine whether climate change, urbanization, or afforestation is the primary driving force of AC.

2. Study areas

The Poyang Lake basin is a typical energy-limited region with $CAI \leq 0.76$. It is a sub-basin of the Yangtze River basin. It was selected as the study area to identify and interpret AC. Five tributaries of the Poyang Lake basin were selected, including the Ganjiang, Fuhe, Xinjiang, Raohe, and Xiushui Rivers (Fig. 1). These tributaries flow through southeastern China, with the drainage areas ranging from 5,013 to 80,948 km^2 and the annual runoff coefficients ranging from 0.44 to 0.64 (Table 1).

3. Datasets and methods

3.1. Datasets

The digital elevation model (DEM) with a 30 m spatial resolution was acquired from the geospatial data cloud (Computer Network Information Center, 2009). Based on this data, the drainage areas of the five study basins were extracted by the hydrology tool of ArcGIS software (version 9.3, manufactured by ESRI, Inc.). The land use map with a 100 m spatial resolution was provided by the Institute of Remote Sensing and Digital Earth, Chinese Academy of Sciences for 1985, 1995, 2000, 2005, and 2010. Annual basin-wide forest coverage rate (FCR) data were collected from the Jiangxi Statistical Yearbook (Bureau of Statistics of Jiangxi, 2012). The monthly normalized difference vegetation index (NDVI) data were obtained from the Ecological Forecasting Lab at the NASA Ames Research Center (Pinzon & Tucker, 2014; 2016). Basin-wide NDVI values were area-weighted averaged to obtain the value in each basin. The monthly streamflow data from 1961 to 2015 were provided by the Jiangxi Provincial Bureau of Hydrology.

The daily meteorological data at each station shown in Fig. 1 were obtained from the China Meteorological Data Sharing Service System. Data quality was controlled with code provided by the National Meteorological Information Center (2019). Stations were excluded when the rate of missing data exceeded 20 %. The meteorological variables included maximum and minimum air temperature (°C), wind speed at 10 m height (m s^{-1}), relative humidity (*RH*, %), sunshine duration (hours), precipitation (mm), solar radiation (R_s, MJ m^{-2} day^{-1}), and E_{pan} (mm day^{-1}) from 1961 to 2015 (Fig. 1). Mean daily temperature (*T*) was the mean value of daily maximum and minimum air

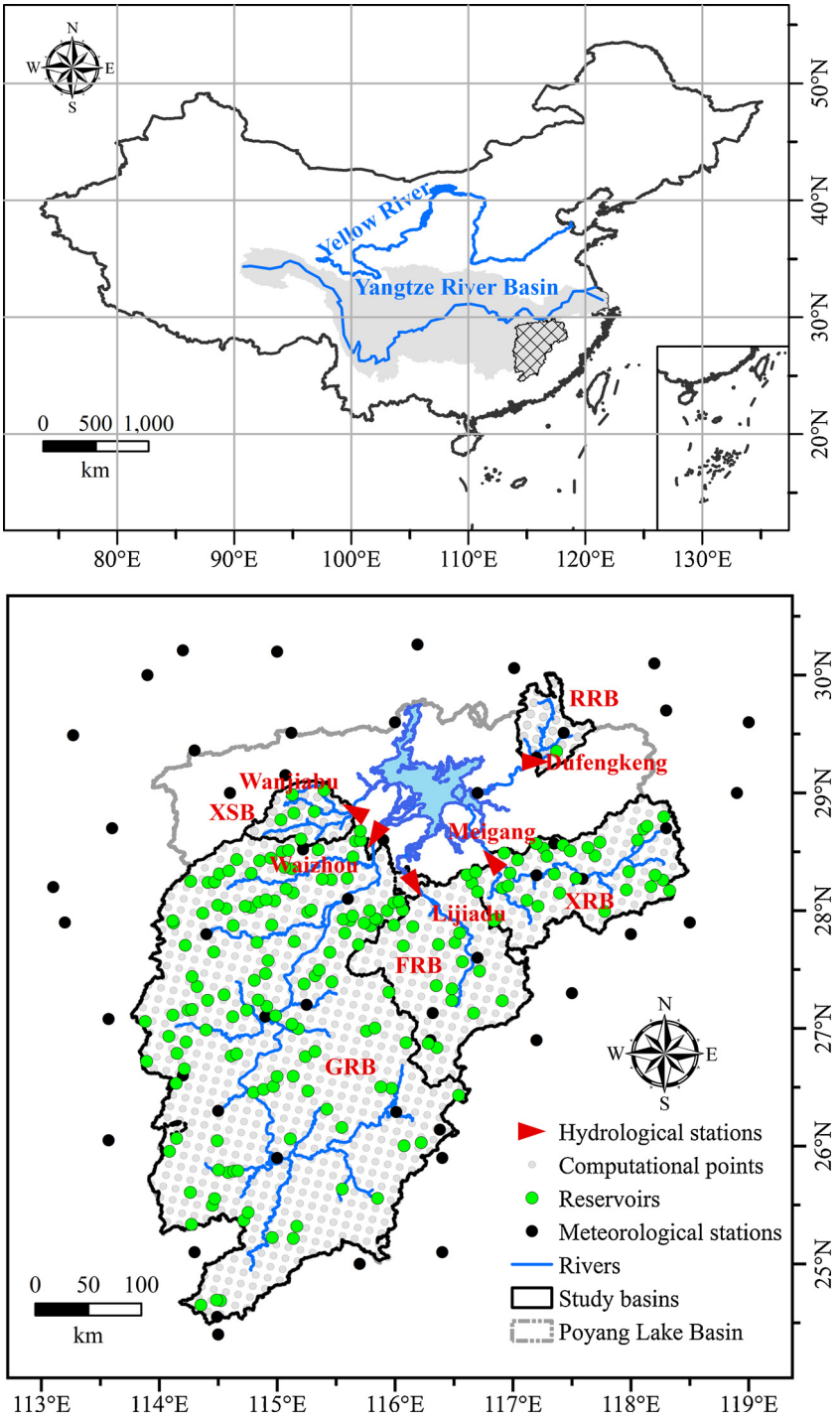

Fig. 1. Study area in southeastrn China including the Ganjiang (GRB), Fuhe (FRB), Xinjiang (XRB), Raohe (RRB), and Xiushui (XSB) River basins, reservoirs, hydro-meteorological stations, and computational grid points.

temperature. Wind speed at 10 m height was adjusted to the wind speed at 2 m height (u_2) (Allen et al., 1998). Among the meteorological stations shown in Fig. 1, observed R_s was only available in three stations.

The procedure to calculate annual evaporation-related meteorological variables, E_{pan}, ET_p, and *WBDE* at the basin scale was as follows:

(1) The gridded study basins

In each study basin, the starting point of the computational grid points was located at the lower left corner of the DEM ASCII file. The spatial interval of the adjacent points in the grid was chosen to be 10 km. The computational grid points (Fig. 1) were generated from the starting point according to the spatial interval using the Meshgrid tool in Matlab R2018b manufactured by MathWorks, Inc, and were clipped to the study basins.

(2) The estimation of annual evaporation-related meteorological variables at meteorological stations

Annual evaporation-related meteorological variables were calculated using daily data at each meteorological station. Observed R_s

Table 1
Basic characteristics of five river basins in southeastern China.

No.	Name	Area (km^2)	Mean annual value (mm)				*RC*
			P	*R*	*WBDE*	ET_p	
1	GRB	80,948	1644	846	798	1015	0.51
2	FRB	15,811	1777	782	995	1009	0.44
3	XRB	15,535	1873	1167	706	1039	0.62
4	RRB	5013	1657	905	752	1010	0.55
5	XSB	3548	1526	982	544	984	0.64

Note: *R* and *RC* represent mean annual runoff depth and runoff coefficient, respectively; *P* is precipitation; *WBDE* is water-budget derived evaporation; ET_p is potential evaporation; GRB, FRB, XRB, RRB, and XSB are the Ganjiang, Fuhe, Xinjiang, Raohe, and Xiushui River basins, respectively.

values were only available at 23 stations over the region defined by 105 − 125 °E and 20 − 35 °N (Table 2). Those stations are named hereafter as solar radiation stations. The A–P Model was employed to estimate R_s at meteorological stations where R_s observations did not exist. Model parameters were calibrated by the ordinary least squares method (OLS) based on the observed R_s and sunshine duration data at each of the solar radiation stations (Angstrom, 1924; Ozturk, 2015). The model estimates of R_s were evaluated by the Nash-Sutcliffe efficiency coefficient (*NSE*) (Nash & Sutcliffe, 1970), coefficient of determination (R^2), and Student's *t*-test (significance level = 0.05) (Gosset, 1942).

(3) The estimation of annual evaporation-related meteorological variables, E_{pan} and ET_p at grid points

Each type of annual data at meteorological or solar radiation stations was interpolated to the grid points using Kriging or Voronoi methods according to the data's probability distribution type (Sarangi, Madramootoo, & Enright, 2006). The Kriging method was applicable to the data obeying a normal distribution. In contrast, the Voronoi method does not require a normal data distribution. The elevations of grid points were extracted from the DEM data by ArcGIS 9.3 software.

We selected 0.23 as the albedo or canopy reflection coefficient (α) (Allen et al., 1998). At each grid point, the annual R_s and net radiation (R_n) were calculated based on gridded sunshine duration (n) and the A–P model parameters (Allen et al., 1998; Angstrom, 1924; Ozturk, 2015) as:

$$R_s = \left(a + b\frac{n}{N}\right)R_a \tag{1}$$

$$R_n = R_{ns} + R_{nl} = (1 - \alpha)R_s + R_{nl} \tag{2}$$

where a and $a+b$ are the fraction of extraterrestrial radiation reaching the earth on overcast days and clear days, respectively, N is the maximum possible sunshine duration (hour), R_a is the extraterrestrial radiation (MJ m^{-2} day^{-1}), R_{ns} is the net solar or shortwave radiation (MJ m^{-2} day^{-1}), and R_{nl} is the net outgoing longwave radiation (MJ m^{-2} day^{-1}).

We then estimated annual ET_p, radiation, and aerodynamic terms of the Penman equation (ET_{pr} and ET_{pa}) (Donohue, McVicar, & Roderick, 2010; Penman, 1948; Shuttleworth, 1993) as:

$$ET_p = ET_{pr} + ET_{pa} \tag{3}$$

$$ET_{pr} = \frac{\Delta}{\Delta + \gamma}R_n = RLH(T)R_n \tag{4}$$

$$ET_{pa} = \frac{\gamma}{\Delta + \gamma}\frac{6430VPD}{\lambda}(1 + 0.536u_2) = ET_{pa}(VPD, T)(1 + 0.536u_2) \tag{5}$$

$$ET_{pa}(VPD, T) = \frac{\gamma}{\Delta + \gamma}\frac{6430VPD}{\lambda} = [1 - RLH(T)]\frac{6430VPD}{\lambda} \tag{6}$$

$$VPD = e_s - e_a = \left(1 - \frac{RH}{100}\right)e_s \tag{7}$$

where Δ is the slope of saturation vapour curve (Pa K^{-1}), γ is the psychrometric constant (Pa K^{-1}), *RLH* is the ratio of latent heat to R_n, *VPD* is the vapor pressure deficit (Pa), λ is the latent heat of vaporization of water (2.45 MJ Kg^{-1}), e_s is the saturation vapor pressure (kPa), and e_a is the actual vapor pressure (kPa).

(4) The estimation of annual evaporation-related meteorological variables, E_{pan}, ET_p, and *WBDE* in the study basins

The gridded annual meteorological variables, E_{pan}, and ET_p were

Table 2
A-P Model parameters and evaluation at solar radiation stations in southeastern China.

No.	Name	LON (°)	LAT (°)	*a*	*b*	N_s	R^2	Student's *t* test value	$t_{0.05}$	*NSE*
1	Zhongshan	113.4	22.5	0.54	0.15	9248	0.77	174	1.96	0.76
2	Guangzhou	113.3	23.1	0.53	0.16	19694	0.82	296	1.96	0.83
3	Shaoguan	113.6	24.8	0.57	0.15	10744	0.82	223	1.96	0.82
4	Ganxian	114.8	25.8	0.55	0.15	19503	0.88	373	1.96	0.88
5	Fuzhou	119.3	26.1	0.59	0.15	19853	0.86	345	1.96	0.86
6	Changning	112.4	26.4	0.60	0.15	8595	0.77	170	1.96	0.77
7	Jianou	118.3	27.1	0.59	0.19	8526	0.79	178	1.96	0.79
8	Changsha	112.9	28.2	0.55	0.14	10485	0.86	256	1.96	0.86
9	Mapoling	113.1	28.2	0.59	0.15	9115	0.86	237	1.96	0.85
10	Jishou	109.7	28.3	0.56	0.14	8690	0.83	205	1.96	0.82
11	Hongjia	121.4	28.6	0.57	0.18	8708	0.87	239	1.96	0.88
12	Nanchang	116.0	28.7	0.57	0.15	19205	0.87	357	1.96	0.86
13	Lushan	116.0	29.6	0.68	0.15	10131	0.84	232	1.96	0.83
14	Tunxi	118.3	29.7	0.59	0.15	8668	0.88	252	1.96	0.89
15	Cixi	121.2	30.3	0.60	0.13	10488	0.88	281	1.96	0.87
16	Hangzhou	120.2	30.3	0.58	0.14	19509	0.85	335	1.96	0.85
17	Wuhan	114.3	30.6	0.53	0.16	18286	0.83	300	1.96	0.81
18	Yichang	111.1	30.7	0.56	0.15	19673	0.83	315	1.96	0.82
19	Baoshan	121.5	31.4	0.55	0.19	8810	0.84	215	1.96	0.86
20	Hefei	117.3	31.9	0.56	0.15	19036	0.85	326	1.96	0.85
21	Nanjing	118.8	32.0	0.57	0.15	19850	0.87	369	1.96	0.87
22	Lvsi	121.6	32.1	0.55	0.16	8751	0.88	248	1.96	0.88
23	Huaian	119.0	33.6	0.54	0.19	5478	0.81	154	1.96	0.84

Note: LON denotes the longitude; LAT denotes the latitude; *a* and *b* denote the parameters of A–P model; N_s denotes the number of samples; R^2 denotes the coefficient of determination; $t_{0.05}$ denotes the critical value of Student's *t*-test value; *NSE* denotes Nash-Sutcliffe efficiency coefficient.

area-weighted averaged to obtain the values in each basin. The *WBDE* was estimated as the difference between the mean annual precipitation in each study basin and streamflow (R) measured at the hydrological stations by neglecting inter-annual variabilities in water storage as:

$$WBDE = P - R \tag{8}$$

The annual *WBDE* time series was restored to the level the reservoirs were at in 1961 (in order to exclude reservoir construction as the driving force of AC) by using the following formulas:

$$\mathrm{WBDE}_i = \mathrm{WBDE}_i + \frac{\sum_{j=1962}^{i}\sum_{k=1}^{NR}(\overline{E_w} - \overline{E_L})[A_{res}(j,k) - A_{riv}(j,k)]}{A_{bsn}} \tag{9}$$

$$\overline{E_L} = \frac{\overline{WBDE} - \overline{E_w}\,\overline{r}}{1 - \overline{r}} \tag{10}$$

$$\overline{E_w} = \frac{\sum_{j=1961}^{2015} K\overline{E_{pan,j}}}{55} \tag{11}$$

where $WBDE_i$ is the *WBDE* for the *ith* year (mm); $\overline{E_w}$ and $\overline{E_L}$ are the mean annual water and land surface evaporation in the study basins, respectively (mm); $A_{res}(j,k)$ is the reservoir area for *jth* year and *kth* reservoir (km^2), estimated by the mean value of the areas corresponding to the reservoir dead and normal storage levels; *NR* is the total number of reservoirs for *jth* year; $A_{riv}(j,k)$ are the original river areas (km^2), estimated by the product of the length of backwater and the width of the terminal of the backwater; A_{bsn} is the basin area (km^2); $\overline{WBDE}$ is the mean annual *WBDE* (mm); $\overline{r}$ is the mean annual area proportion of water bodies, estimated by the land use maps; $\overline{E_{pan,j}}$ is the E_{pan} for *jth* year in the study basin; and K is a conversion coefficient (Fu et al., 2004).

3.2. Methods

(1) Changes in annual evaporation-related meteorological variables

Trends of annual evaporation-related meteorological variables were detected by ordinary linear regression (OLR) (Zhang, Liu, Xu, Xu, & Jiang, 2006) in terms of R_n, T, u_2, RH, and P. One-sample ordinary Student's t-test was applied to evaluate the trends (significance level = 0.05) (Gosset, 1942).

(2) The abnormal correlation between *AED* and *AE*

AED usually shows a positive correlation with *AE* in Yangtze River basin (Wang et al., 2011). In the study basins, the trends in annual ET_p and E_{pan} were detected by OLR and Student's t-test to reveal any temporal trends in *AED* (significance level = 0.05) (Gosset, 1942). Their change points were further assessed by the Pettitt method (Gao, Mu, Wang, & Li, 2011; Pettitt, 1979) at the same significance level. The trends in annual *WBDE* were similarly detected to reveal any temporal trends in *AE*. Nonpositive correlations between *AED* and *AE* were identified if the trends of annual *AED* and *AE* were inconsistent from each other. Compared with the overall positive correlation in the Yangtze River Basin, the detected nonpositive correlations in the study basin were applied to verify the observed AC.

(3) Driving force of the abnormal correlation between *AED* and *AE*

The driving force of AC was identified in three steps. Firstly, the temporal change in *AED* was attributed to changes in meteorological variables according to the sensitivity method of the Penman equation (Donohue et al., 2010). Secondly, the observed temporal change in *AE* was attributed to climate change and human activities according to the decomposition method of the Budyko equation (Wang & Hejazi, 2011). Lastly, both attribution analyses were integrated to explore the impacts of climate change and human activities on AC in order to identify the primary driving force.

a Attribution of the temporal change in *AED* to climate change

The temporal changes in mean annual ET_p, ET_{pa}, and ET_{pr} (ΔET_p, ΔET_{pa}, and ΔET_{pr}) were calculated between the two adjacent periods separated by the change point of annual ET_p. These changes were further quantitatively attributed to changes in the meteorological variables using the sensitivity method of the Penman equation during the same period (Donohue et al., 2010), shown as follows:

$$\Delta ET_p = \Delta ET_{pr} + \Delta ET_{pa} \tag{12}$$

$$\Delta ET_{pr} = \int_{A_0}^{A_1} \frac{\partial ET_{pr}}{\partial \Delta}\frac{d\Delta}{dT}dT + \int_{A_0}^{A_1} \frac{\partial ET_{pr}}{\partial R_n}dR_n \tag{13}$$

$$\Delta ET_{pa} = \int_{A_0}^{A_1}\left(\frac{\partial ET_{pa}}{\partial \Delta}\frac{d\Delta}{dT} + \frac{\partial ET_{pa}}{\partial e_s}\frac{de_s}{dT} + \frac{\partial ET_{pa}}{\partial e_a}\frac{\partial e_a}{\partial T}\right)dT + \int_{A_0}^{A_1}\frac{\partial ET_{pa}}{\partial u_2}du_2 + \int_{A_0}^{A_1}\frac{\partial ET_{pa}}{\partial e_a}\frac{\partial e_a}{\partial RH}dRH \tag{14}$$

where A refers to the variable sets that include T, u_2, R_n, and RH. Corresponding subscripts 0 and 1 denote the states of A in the periods before and after the change point of *AED*, respectively.

The contribution rates of ΔR_n, ΔT, Δu_2, and ΔRH on ΔET_p were estimated by the ratio of the corresponding partial integral to ΔET_p. The contribution rates on ΔET_{pr} and ΔET_{pa} were similarly estimated (Chu et al., 2017; Donohue et al., 2010; Ning, Li, Liu, & Han, 2016).

b Attribution of the temporal change in *AE* to climate change and human activities

The Budyko framework is a semi-empirical model used to quantify the water-energy balance under certain climate regions. Fu's equation is the analytical solution to the framework (Fu, 1981; Yang et al., 2007) with parameter ω, describing the relationship between *AED/P* and *AE/P* (φ), and given as:

$$\varphi = f\left(\frac{AED}{P},\omega\right) = 1 + \frac{AED}{P} - \left[1 + \left(\frac{AED}{P}\right)^{\omega}\right]^{\frac{1}{\omega}} \tag{15}$$

Parameter ω is related to the geobotanic zonality types (Cai et al., 2014), which can be changed by human activities. Annual ω was calibrated based on observed φ (φ_o) and simulated φ (φ_s) according to OLS with relative error less than 5%, shown as follows:

$$\min z = (\varphi_s - \varphi_o)^2 = \left\{1 + \frac{AED}{P} - \left[1 + \left(\frac{AED}{P}\right)^{\omega}\right]^{\frac{1}{\omega}} - \varphi_o\right\}^2 \tag{16}$$

Calibrated annual ω was temporally averaged in the periods before the change point of *AED* (ω_1) and after the point (ω_2). Budyko curves were drawn according to Fu's equation, ω_1 and ω_2 in these two periods (Fig. 2). Suppose the river basin has temporally shifted from Point S_1 (prechange period) to Point S_3 (postchange period). The φ and P in the prechange period was denoted as φ_{S_1} and P_{S_1}, which was changed into φ_{S_3} and P_{S_3} in the postchange period. The observed change in *AE* was assessed as (Wang & Hejazi, 2011):

$$\Delta AE_o = \varphi_{S_3}P_{S_3} - \varphi_{S_1}P_{S_1} \tag{17}$$

The river basin would change from Point S_1 to Point S_2 along the curve obeying Fu's equation, only driven by climate change (Fig. 2) (Wang & Hejazi, 2011). The φ and P at the Point S_2 were denoted as φ_{S_2} and P_{S_2}, respectively. The difference of the φ_{S_2} and φ_{S_1} was the climate change-induced change in φ, recorded as $\Delta\varphi_c$ (Wang & Hejazi, 2011). Then the climate change-induced change in *AE* (ΔAE_c) was calculated

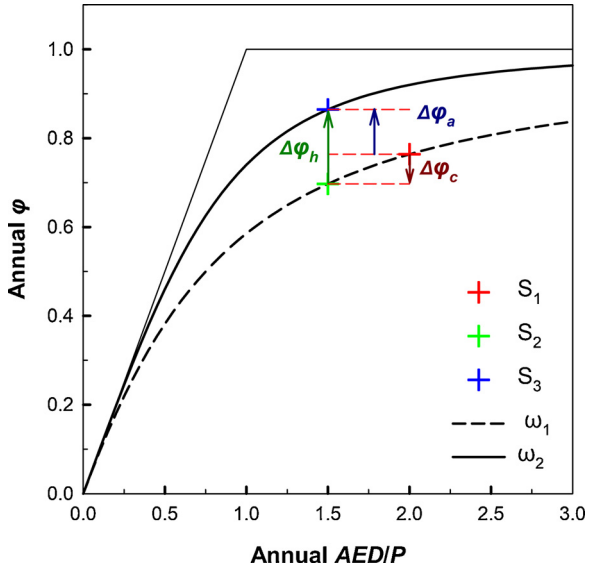

Fig. 2. Attributions of climate change and human activities to the change in annual φ according to Fu's equation.
Note: φ is the ratio of actual evaporation to precipitation; P is precipitation; AED represents atmospheric evaporation demand; ω_1 and ω_2 represent the parameters of Fu's equation before and after the change point of AED, respectively; S_1 and S_3 are the points characterized by the mean annual AED/P and ω before and after the change point of AED, respectively; S_2 is the point characterized by the mean annual AED/P after the change point of AED and ω_1.

as:

$$\Delta AE_c = \varphi_{S_2} P_{S_2} - \varphi_{S_1} P_{S_1} \quad (18)$$

The difference of the φ_{S_3} and φ_{S_2} was the human activities-induced change in φ, recorded as $\Delta\varphi_h$ (Wang & Hejazi, 2011). Then the human activities-induced change in AE (ΔAE_h) was calculated as:

$$\Delta AE_h = \varphi_{S_3} P_{S_3} - \varphi_{S_2} P_{S_2} \quad (19)$$

c Driving force of the abnormal correlation between AED and AE

Responses of temporal changes in AED and AE to climate change were revealed by combining the quantitative contribution rates of climate change on ΔET_p with ΔAE_c. In contrast, the response to human activities was detected by combining the influence of human activities on ΔET_p with ΔAE_h. Both responses were integrated to determine why the AC appeared and then to identify its driving force. In addition, the annual area proportions of different land use types were compared to find the temporal-spatial distribution of land use during 1985–2010. The temporal changes in the annual FCR and NDVI were assessed to identify changes in land cover. The changes in land use and land cover were summarized to identify the main types of human activities. The detected main human activity was the primary driving force of AC, if the human activities were confirmed as the driving force.

4. Results

4.1. Changes in annual evaporation-related meteorological variables

4.1.1. A–P Model parameters at meteorological stations

Table 2 shows the calibrated A–P Model parameters (a and b) and evaluation at solar radiation stations. The parameters a and b ranged from 0.53 to 0.68 and 0.13 to 0.19, spatially averaged to be 0.57 and 0.16, respectively. The mean NSE value between the simulated and observed R_s was 0.85. And the Student's t-test value was greater than its critical value ($t_{0.05}$) at each station. Accordingly, the simulation of R_s by the A–P model was considered to be acceptable.

Table 3 shows the interpolated A–P Model parameters at meteorological stations that did not have observed R_s using the Kriging method. The parameters a and b ranged from 0.53 to 0.66 and from 0.15 to 0.18, spatially averaged to be 0.58 and 0.16, respectively.

4.1.2. Trends of annual evaporation-related meteorological variables

Fig. 3 shows the temporal trends of basin-wide annual meteorological variables. Annual R_n, RH, and u_2 decreased significantly in all study basins at tendency rates ranging from -0.14 to -0.11 MJ m^{-2} day^{-1} decade^{-1}, −0.6 % to −0.4 % decade^{-1}, and -0.16 to -0.10 m s^{-1} decade^{-1}, respectively. In contrast, annual T increased significantly at tendency rates ranging from 0.17 to 0.28 °C decade^{-1} depending on the different basins. Meanwhile, annual P exhibited no trend. The only exception to

Table 3
A-P Model parameters at meteorological stations that did not have observed R_s in southeastern China.

No.	Name	LON (°)	LAT (°)	a	b	No.	Name	LON (°)	LAT (°)	a	b
1	Lianping	114.5	24.4	0.54	0.16	25	Yifeng	114.5	28.2	0.59	0.15
2	Longnan	114.5	24.6	0.54	0.15	26	Shangrao	117.6	28.3	0.59	0.18
3	Xunwu	115.7	25.0	0.53	0.17	27	Guixi	117.2	28.3	0.58	0.17
4	Nanxiong	114.3	25.1	0.56	0.15	28	Jingan	115.2	28.5	0.58	0.15
5	Shanghang	116.4	25.1	0.53	0.17	29	Dexing	117.4	28.6	0.59	0.17
6	Changting	116.4	25.9	0.54	0.17	30	Pingjiang	113.6	28.7	0.59	0.15
7	Guidong	113.6	26.1	0.59	0.15	31	Yushan	118.3	28.7	0.59	0.17
8	Ninghua	116.4	26.1	0.54	0.17	32	Xiushui	114.6	29.0	0.59	0.15
9	Ningdu	116.0	26.3	0.54	0.16	33	Poyang	116.7	29.0	0.61	0.15
10	Suichuan	114.5	26.3	0.57	0.15	34	Quzhou	118.9	29.0	0.59	0.16
11	Jiangganshan	114.2	26.6	0.58	0.15	35	Wuning	115.1	29.2	0.61	0.15
12	Guangchang	116.3	26.9	0.55	0.17	36	Jingdezhen	117.2	29.3	0.62	0.15
13	Taining	117.2	26.9	0.56	0.18	37	Gangkou	114.3	29.4	0.58	0.15
14	Lianhua	113.6	27.1	0.59	0.15	38	Honghu	113.3	29.5	0.55	0.15
15	Jianxian	114.9	27.1	0.56	0.15	39	Yangxin	115.1	29.5	0.62	0.15
16	Nanfeng	116.3	27.1	0.55	0.17	40	Qimen	117.4	29.5	0.62	0.15
17	Yongfeng	115.3	27.2	0.56	0.15	41	Chunan	119.0	29.6	0.59	0.15
18	Shaowu	117.5	27.3	0.57	0.18	42	Jiayu	113.9	30.0	0.54	0.16
19	Nancheng	116.7	27.6	0.56	0.17	43	Dongzhi	117.0	30.1	0.66	0.15
20	Yichun	114.4	27.8	0.59	0.15	44	Huangshan	118.2	30.1	0.59	0.15
21	Wuyishan	118.0	27.8	0.58	0.18	45	Huangshi	115.0	30.2	0.60	0.15
22	Zhuzhou	113.2	27.9	0.59	0.15	46	Jiangxia	114.2	30.2	0.54	0.16
23	Pucheng	118.5	27.9	0.59	0.18	47	Heta	116.2	30.3	0.66	0.15
24	Zhangshu	115.6	28.1	0.56	0.15						

Note: LON denotes the longitude; LAT denotes the latitude; a and b denote the parameters of A–P model.

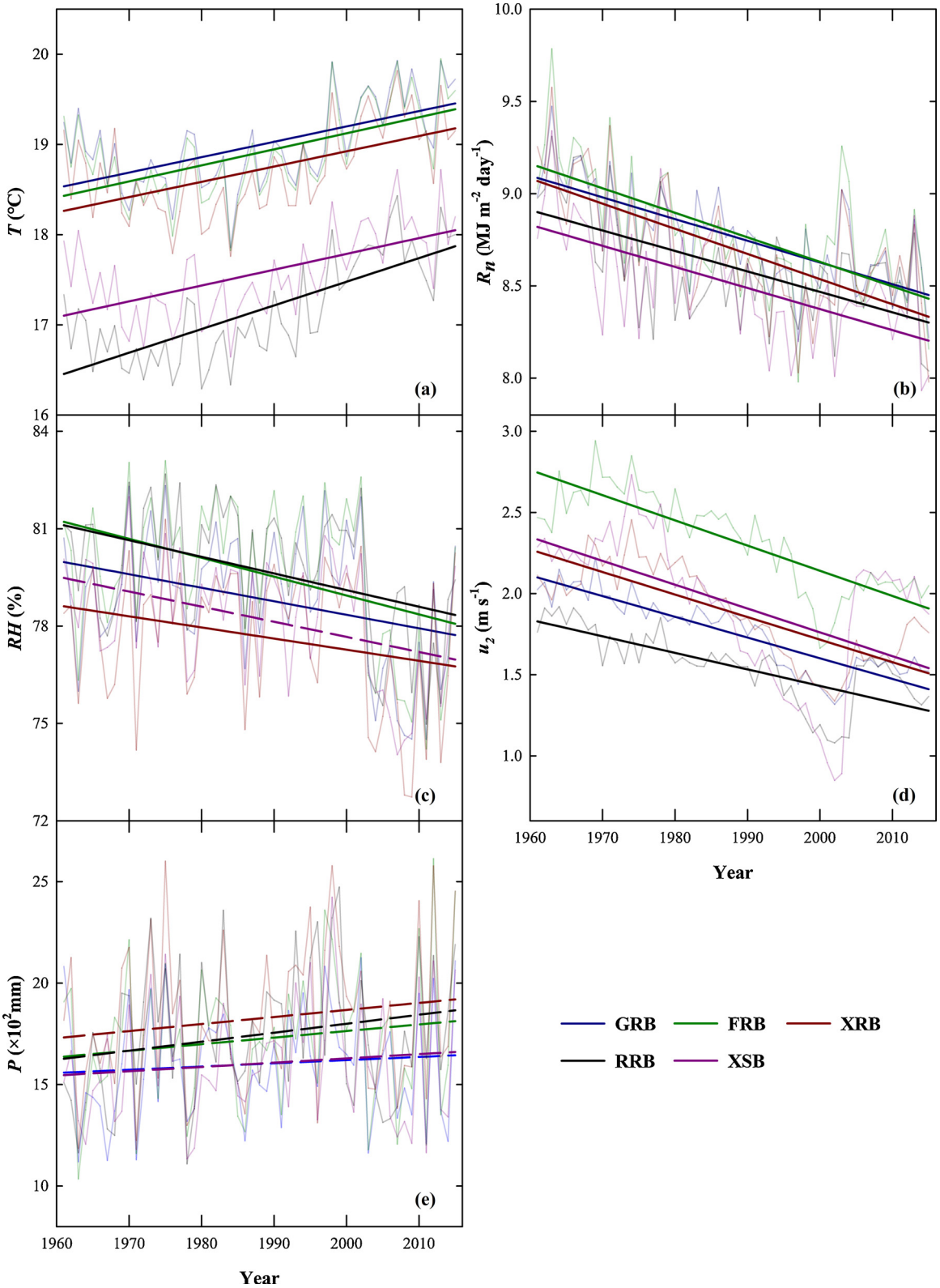

Fig. 3. Annual variation of spatially averaged values of (a) temperature (*T*), (b) net radiation (R_n), (c) relative humidity (*RH*), (d) wind speed (u_2), and (e) precipitation (*P*) in five river basins in southeastern China. (GRB, Ganjiang; FRB, Fuhe; XRB, Xinjiang; RRB Raohe; and XSB, Xiushui River basins).
Note: solid lines denote significant temporal trends; dashed lines denote nonsignificant temporal trends.

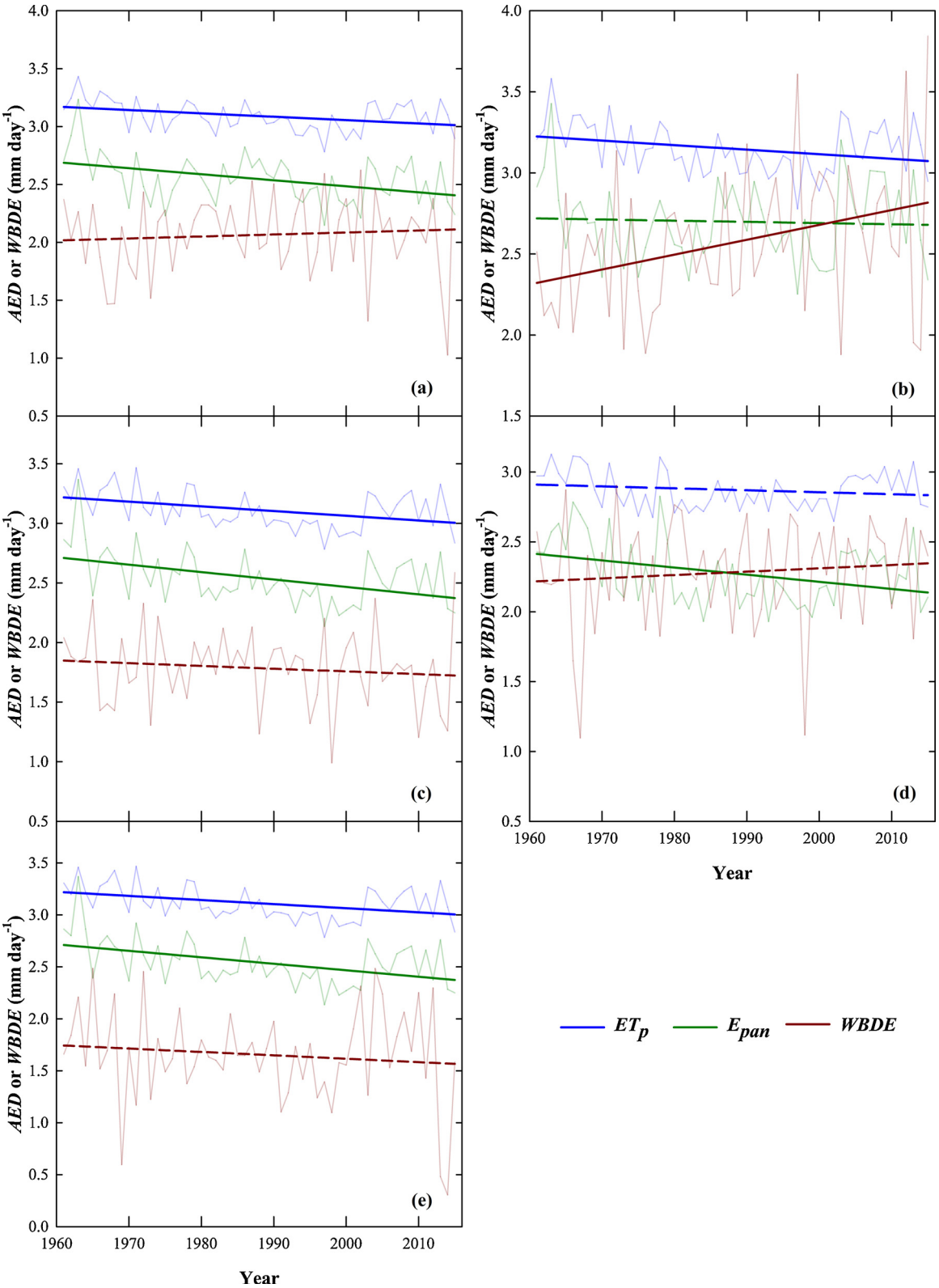

Fig. 4. Annual variation of spatially averaged values of potential evaporation (ET_p), pan evaporation (E_{pan}), and water budget-derived evaporation (*WBDE*) in river basins in southeastern China.
Note: the panel letters (a, b, c, d, and e) represent Ganjiang (GRB), Fuhe (FRB), Xinjiang (XRB), Raohe (RRB), and Xiushui (XSB) River basins, respectively; solid lines denote significant temporal trends; dashed lines denote nonsignificant temporal trends.

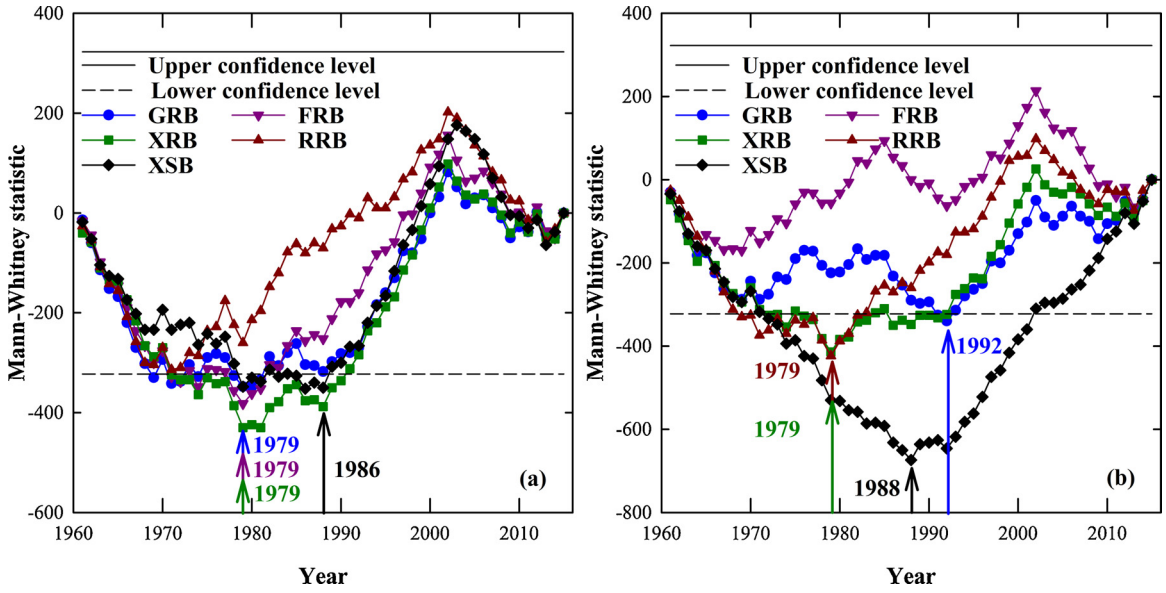

Fig. 5. Change points of annual pan evaporation (E_{pan}, a) and potential evaporation (ET_p, b), in southeastern China. (GRB, Ganjiang; FRB, Fuhe; XRB, Xinjiang; RRB, Raohe; and XSB, Xiushui River basins).

these trends was that the Student's *t*-test value for annual *RH* in XSB was less than the critical value, meaning that no significant trend was detected in that case.

4.2. The abnormal correlation between AED and AE

Fig. 4 shows the temporal trends of basin-wide annual *AED* and *AE*. Annual ET_p decreased significantly in all study basins except *RRB* at tendency rates ranging from -0.04 to -0.03 mm day^{-1} decade^{-1}. Annual E_{pan} decreased significantly in all study basins except *FRB* at tendency rates ranging from -0.12 to -0.06 mm day^{-1} decade^{-1}. In contrast, annual *WBDE* increased in FRB at a tendency rate of 0.09 mm day^{-1} decade^{-1} and remained constant in other study basins (Fig. 4). The trends between *AED* and *AE* were different from each other. The observed spatial AC was verified. In addition, the slope value of the temporal trends of *AED* and *AE* tended to be smaller in GRB, FRB, and XRB after 1979 (see Supplementary Fig. 1 and 2). Temporal AC was also verified in these basins.

Fig. 5 shows the change points of annual *AED*. The maximum absolute values of annual ET_p's Mann–Whitney statistics appeared in 1979, 1979, 1979, and 1986 in GRB, FRB, XRB, and XSB respectively, lying outside the confidence interval. These years were the change points of annual ET_p. In comparison, the change points of annual E_{pan} were similarly determined to be 1992, 1979, 1979, and 1988 in GRB, XRB, RRB, and XSB, respectively. The majority of the change points for both annual ET_p and E_{pan} occurred in 1979.

4.3. Driving force of the abnormal correlation between AED and AE

4.3.1. Attribution of the temporal change in AED to climate change

Fig. 6 shows the contributions of the temporal changes in meteorological variables on the ΔET_{pr}, ΔET_{pa}, and ΔET_p in the study basins. Increasing *T* contributed -33 % to -11 % to the decrease in ET_{pr} (Fig. 6a) by increasing the *RLH* (Supplementary Fig. 3). Conversely, the decreasing R_n contributed 111 %–133 % to the decrease in ET_{pr}. Accordingly, an increased proportion of latent heat relative to R_n was insufficient to compensate for the decrease in ET_{pr} induced by decreasing R_n, and as such ET_{pr} decreased.

Decreasing *RH* and increasing *T* contributed -126 % to -18 % and -59 % to -11 % to the decrease in ET_{pa} in the study basins, respectively (Fig. 6b). Conversely, deceasing u_2 contributed 128 %–284 % to the decrease in ET_{pa}. Accordingly, the influence of decreasing *RH* and increasing *T* was totally offset by the influence of the decreasing u_2 to make annual ET_{pa} constant, indicated by no trend detected (Supplementary Fig. 3).

Decreasing R_n and u_2 contributed from 66 % to 110 % and 40%–70% to the decrease in ET_p, respectively. Conversely, decreasing *RH* and increasing *T* contributed from -21 % to -6% and -37 % to -11 % to the decrease in ET_p, respectively. Accordingly, decreasing R_n and u_2 produced larger variation in ET_p.

4.3.2. Attribution of the temporal change in AE to climate change and human activities

Fig. 7 shows the contributions of climate change and human activities to the $\Delta\varphi_o$ based on Fu's equation. Mean annual equation parameter ω increased from 2.02 before 1979 to 2.32 after 1979 in GRB, in addition to 2.52–3.23 in FRB, 1.68–1.72 in XRB, and 2.55–2.83 in RRB (Fig. 7a). In contrast, mean annual ω decreased slightly from 1.82 to 1.76 in XSB. The Budyko curves were substantially higher after 1979 than the Budyko curves before 1979 in GRB, FRB, XRB and RRB (Fig. 7b) except in XSB.

Negative $\Delta\varphi_c$ and ΔAE_c values were detected, ranging from -0.057 to -0.025 and -22 to -17 mm respectively, depending on the different basins (Fig. 7c). The spatially averaged ΔAE_c was -20 mm in the study basins. In contrast, positive $\Delta\varphi_h$ and ΔAE_h values were observed in four of the five river basins, ranging from 0.01 to 0.05 and 40 to 141 mm respectively, depending on the different basins. Negative $\Delta\varphi_h$ was only observed in XSB. The corresponding ΔAE_h value was confirmed to be -5 mm. The spatially averaged ΔAE_h was 78 mm in the study basins. Accordingly, the overall climate change-induced decrease and the human activities-induced increase in *AE* was verified.

4.3.3. Driving force of the abnormal correlation between AED and AE

Decreasing R_n and u_2 were the major climate factors reducing *AED*. These reductions also led to a 20 mm decrease in mean annual *AE* in the study basins. Climate change led to the simultaneous temporal decrease in *AED* and *AE*. Human activities resulted in an increase of 78 mm in mean annual *AE* but had no effect on *AED*. Eventually, annual *AED* decreased, but annual *AE* did not appear to exhibit the same temporal trend. So overall, human activities appear to be the driving force of AC.

Fig. 8 shows the temporal-spatial distribution of land use and cover. The forest land and arable land accounted for 62.7 % and 26.1 % of the

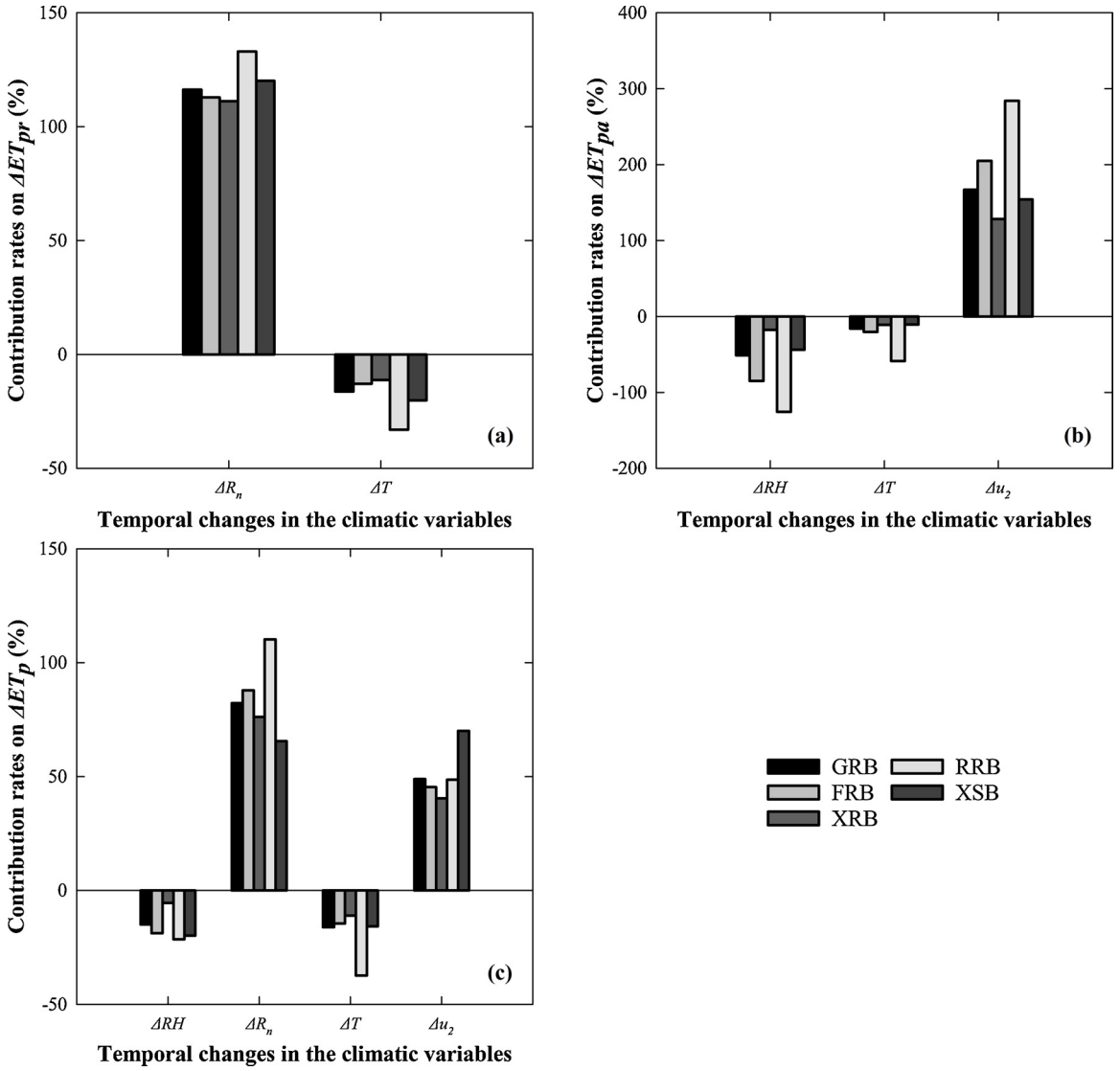

Fig. 6. Contribution rates of the temporal changes in meteorological variables to changes in (a) radiation fraction of Penman potential evaporation (ET_{pr}), (b) aerodynamic fraction of Penman potential evaporation (ET_{pa}) and (c) Penman potential evaporation (ET_p) in river basins in southeastern China.
Note: GRB, FRB, XRB, RRB, and XSB are the Ganjiang, Fuhe, Xinjiang, Raohe, and Xiushui River basins, respectively; ΔRn, ΔT, ΔRH, and Δu_2 denote the temporal changes in net radiation, temperature, relative humidity, and wind speed respectively.

terrestrial surface, respectively. These two land use types remained constant during the period from 1985 to 2010, indicated by relatively small standard errors. Accordingly, the forest and arable land were the main land use types. Additionally, both of the annual FCR and NDVI simultaneously and dramatically increased around 1980. Arable land consisted mainly of double-cropping paddy fields, whose NDVI fluctuated during half-year periods rather than multi-year periods. Therefore, the growth of paddy areas could not cause the observed temporal increase in annual NDVI. So, the observed increase in NDVI and FCR was a result of afforestation. Accordingly, afforestation was the main human activity leading to the abnormal correlation between *AED* and *AE* rather than urbanization and climate change.

5. Discussion

This study focused on identifying and interpreting the AC between *AED* and *AE* in the energy-limited region of southeastern China. Afforestation was determined to be the major human activity that likely explains the observed AC. During this analysis process, we quantitatively established the integrated response chain from climate change and afforestation to the temporal change in *AE*.

5.1. Changes in annual evaporation-related meteorological variables

Meteorological states are regulated by both local water-energy processes and large-scale climate conditions. In the five river basins used in this study, the large-scale climate conditions were especially important. Specifically, decreasing R_n and u_2 are the likely consequence of radiative dimming (Cohen, Ianetz, & Stanhill, 2002; Liu et al., 2004; Papaioannou, Kitsara, & Athanasatos, 2011; Roderick & Farquhar, 2002; Wild, Ohmura, Gilgen, & Rosenfeld, 2004) and wind stilling (McVicar, Roderick, Donohue, Li et al., 2012; Roderick, Rotstayn, Farquhar, & Hobbins, 2007), respectively. Increasing annual temperature was consistent with global warming that is induced by increasing concentrations of greenhouse gases in the atmosphere (Milly & Dunne, 2016; Tsai, 2017; Vallis, Zurita-Gotor, Cairns, & Kidston, 2015). Annual precipitation showed no trend in the study basins, similar to overall trends in the Yangtze River basin (Ukkola & Prentice, 2013).

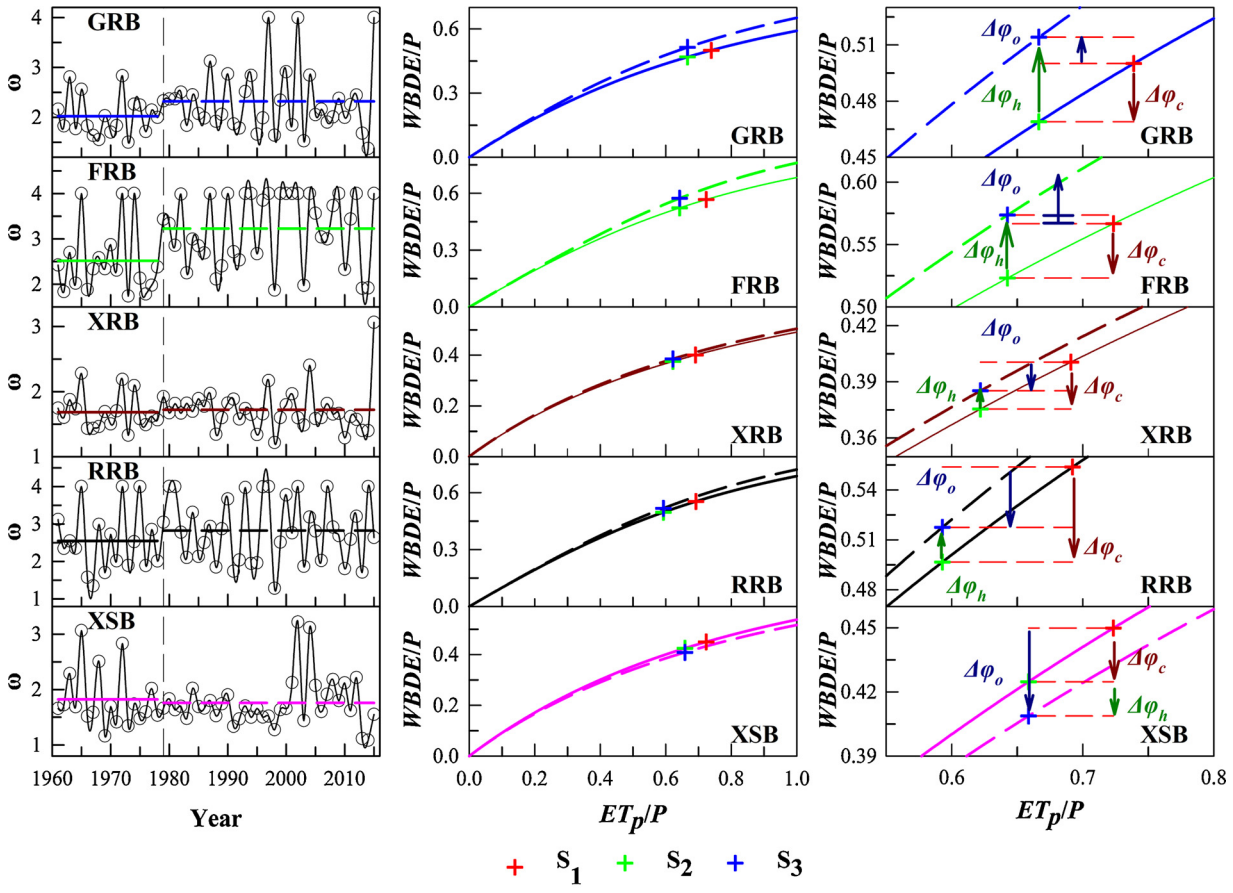

Fig. 7. Quantitative attributions on $\Delta\varphi_o$ based on Fu's equation.
Note: the solid lines and dashed lines in each panel denote the periods before and after 1979, respectively; GRB, FRB, XRB, RRB, and XSB are the Ganjiang, Fuhe, Xinjiang, Raohe, and Xiushui River basins, respectively; ω represents the parameter of Fu's equation; *P* is precipitation; *WBDE* is water-budget derived evaporation; *ETp* is potential evaporation; $\Delta\varphi_o$, $\Delta\varphi_c$, and $\Delta\varphi_h$ are the observed, climate change-induced and human activities-induced ratio of actual evaporation to precipitation, respectively; S_1 and S_3 are the points characterized by the mean annual *ETp/P* and ω before and after the change point of *AED*, respectively; S_2 is the point characterized by the mean annual *AED/P* after the change point of *AED* and ω before the point.

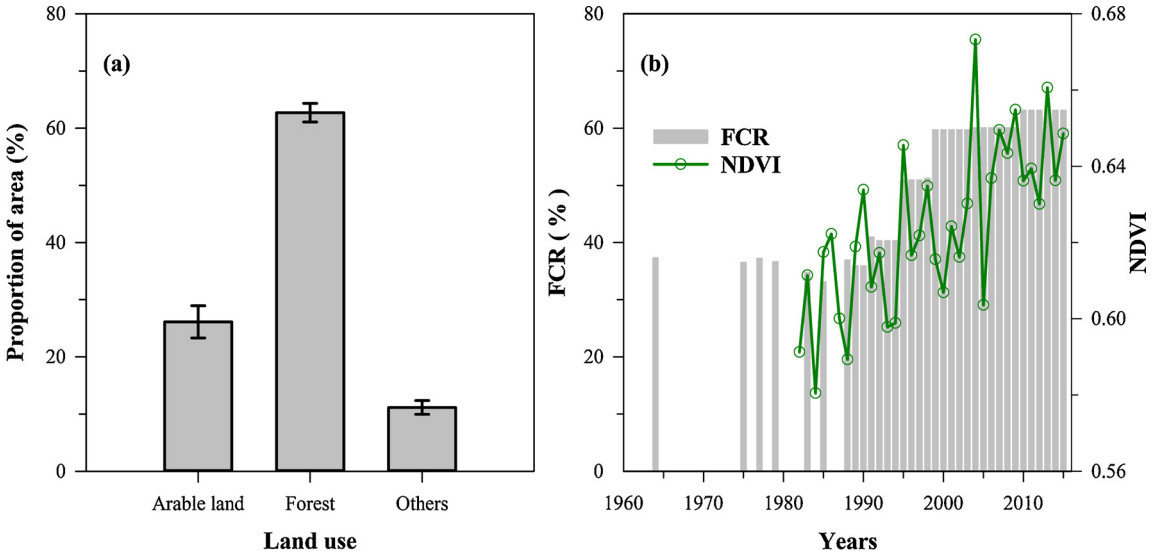

Fig. 8. Spatial framework and temporal changes of land use and cover. FCR, forest cover rate; NDVI, normalized difference vegetation index. The error bars are the standard errors of the means.

5.2. The abnormal correlation between AED and AE

Study basins are an intermediate-scale region. At such a scale, a stable correlation between *AED* and *AE* can be expected by eliminating the impact of the micro-topography. The driving forces of AC are restricted to climate change and human activities rather than the spatial distribution of the micro-topography. Specifically, at smaller spatial scales, diverse correlations between *AED* and *AE* may be detected. This diversity may be regulated more by the complicated spatial distribution of micro-topography. However, as the spatial scale under consideration is expanded, such diversities are possibly masked such that a single type of correlation between *AED* and *AE* is observed. With scale expansion, the influence of microtopography on the correlation gradually becomes weaker. Under this condition, a stable correlation represents the interacting effects of local climate and terrestrial land surface condition on the hypothesis of no effect of human activities. The AC can be attributed to climate and human activities-induced terrestrial land surface changes.

AED decreased in the study basins, as indicated by ET_p and E_{pan}. This finding was consistent with overall temporally decreasing trends of *AED* in the world mentioned above. However, a significant change point for *AED* occurred in 1979 when *AED* began to decrease. After 1979, the study basins also experienced strong afforestation. This was suspected as the driving force causing the existence of the change point.

AC between *AED* and *AE* was confirmed for the study basins presented in this paper. In humid regions, the observation and simulation on the AC have been reported for areas with dense forests (Carmona et al., 2016; Lawrimore & Peterson, 2000). Perhaps the areas of these previous studies experienced similar afforestation as occurred in our study basins. This supposition needs to be further verified.

5.3. Driving force of the abnormal correlation between AED and AE

Local hydrological processes and large-scale climate conditions are the key variables regulating negative and positive correlation between *AED* and *AE*, respectively. Specifically, an arid region was typically far away from oceans. This region can be likened to a relatively enclosed room with little outside influence. The changes in water-energy flows during the local hydrological process, indicated by the changes in *AE*, may effectively alter the local climate. During this process, the *AED* changed through inverse trends of *AE*, which can be understood as a compensation mechanism for *AE* changes according to BCH (Bouchet, 1963). This compensation mechanism was more significant in arid regions because of strong local interaction. Consequently, the negative correlation between *AED* and *AE* was easily seen in this region. In contrast, the humid region was closer to the ocean. The correlation was regulated by large-scale climate conditions. The impact of local water-energy processes on the correlation between *AED* and *AE* was relatively limited and easily offset by large-scale climate conditions. For this situation, the positive correlation was easily observed in this region.

Afforestation strengthened the local hydrological process, thus driving the correlation between *AED* and *AE* to tend to be negative. Specifically, the study basins were typically energy-limited regions, where the decrease in *AE* was expected as a result of decreasing *AED*. However, the regional afforestation increased the ω parameter of Fu's equation and the ratio of *AE* to *AED*. This afforestation-induced elevated ratio offset the expected decrease in *AE* against the impact of decreasing *AED*. It produced the inconsistent temporal trends between *AED* and *AE* through converting more atmospheric evaporation energy into actual one, which strengthened the local hydrological process. As a result, the correlation between *AED* and *AE* tended to be negative.

Accurate assessment of land use and coverage changes (LUCC) requires integration of changes in land use maps and vegetation canopy data. However, current simulations of streamflow or evaporation typically consider only either land use maps or a vegetation canopy change index, such as NDVI or leaf area index (Guo, Hu, & Jiang, 2008; Yan et al., 2013). Consequently, understanding LUCC may sometimes be uncertain. There may also be unknown genetic effects on changes in water-energy flows. Combining land use maps with vegetation canopy change indices may be a better way to understand LUCC (Ye, Zhang, Bai, & Hu, 2011).

6. Conclusion

We assessed the temporal changes in the meteorological variables, *AED,* and *AE* by ordinary linear regression and by the Pettitt method for five energy-limited basins in southeast China. The temporal trends between *AED* and *AE* were compared to explore whether the abnormal correlations appeared in the study basins relative to the Yangtze River basin. The driving forces of the abnormal correlation were identified as being either climate change or human activities using the sensitivity method of the Penman equation and the decomposition method of the Budyko equation.

Annual R_n, u_2, and *RH* were found to decrease significantly at tendency rates ranging from -0.14 to -0.11 MJ m^{-2} day^{-1} $decade^{-1}$, -0.6 % to -0.4 % $decade^{-1}$, and -0.16 to -0.10 m s^{-1} $decade^{-1}$, respectively. Conversely, annual *T* increased significantly at tendency rates ranging from 0.17 to 0.28 °C $decade^{-1}$. Meanwhile, annual *P* was found to have no trend.

Generally, *AED* showed a positive correlation with *AE* in the Yangtze River basin. Annual ET_p and E_{pan} decreased significantly at tendency rates ranging from -0.04 to -0.03 and -0.12 to -0.06 mm d^{-1} $decade^{-1}$, respectively. Their change points both occurred in 1979. Accordingly, annual *AED* decreased after 1979. In comparison, *AE* increased significantly at a tendency rate of 0.09 mm d^{-1} $decade^{-1}$ in FRB and remained constant in other study basins, as indicated by *WBDE*. Nonpositive correlation between *AED* and *AE* appeared and AC was verified compared with the Yangtze River basin.

The increasing *T* contributed −33 % to −11 % to the decrease in ET_{pr} by increasing the proportion of latent heat to R_n in the study basins. This increased proportion of latent heat cannot compensate for the decrease in ET_{pr} induced by a reduction in R_n, the contribution rates of which ranged from 111 %–133 %. Eventually, annual ET_{pr} decreased significantly at tendency rates ranging from −0.03 to −0.018 mm day^{-1} $decade^{-1}$. In addition, decreasing *RH* and increasing *T* contributed −126 % to −18 % and −59 % to −11 %, respectively, to the decrease in ET_{pa} by increasing *VPD*. This influence was totally offset by of the influence of decreasing u_2, the contribution rates of which ranged from 128 %–284 %. There was, consequently, no temporal trend detected in ET_{pa}. Meanwhile, decreasing R_n and u_2 contributed most to the decrease in ET_p, with contribution rates ranging from 66 % to 110 % and 40 %–70 %, respectively. Accordingly, decreasing R_n and u_2 were the major climate factors in reducing *AED*.

Climate change also led to the simultaneous decrease of 20 mm in mean annual *AE* in the study basins. However, human activities had no effect on *AED* and resulted in an increase of 78 mm in mean annual *AE*. Eventually annual *AED* decreased, but annual *AE* did not exhibit the same temporal trend. Accordingly, afforestation was the main human activity changing the correlation between *AED* and *AE* (rather than urbanization and climate change).

Acknowledgement

The contribution of Xingmin Mu and Guangju Zhao presents the proposed hypothesis and design of the research framework. Hua Bai are responsible for the data analysis, followed by writing paper, sponsored by Science and Technology Project for the Education Department of Jiangxi Province (GJJ171005) and the key program for the Jiangxi Provincial Hydraulic Science and Technology Projects (KT201726). Xiaoxiao Yang and Jianchu Huang are responsible for the data collection and quality control. This paper is revised by Xianghui Lu, Chao Yue and Faliang Gui.

Appendix A. Supplementary data

Supplementary material related to this article can be found, in the online version, at doi:https://doi.org/10.1016/j.scs.2020.102075.

References

Abtew, W., Obeysekera, J., & Iricanin, N. (2010). Pan evaporation and potential evapotranspiration trends in South Florida. *Hydrological Processes, 25*(6), 958–969. https://doi.org/10.1002/hyp.7887.

Ali, A. M., Shafiee, M. E., & Berglund, E. Z. (2017). Agent-based modeling to simulate the dynamics of urban water supply: Climate, population growth, and water shortages. *Sustainable Cities and Society, 28*, 420–434. https://doi.org/10.1016/j.scs.2016.10.001.

Allen, R. G., Pereira, L. S., Raes, D., & Smith, M. (1998). *Crop evapotranspiration-Guidelines for computing crop water requirements.* FAO Irrigation and Drainage Paper, 56Rome: FAO.

Angstrom, A. (1924). Solar and terrestrial radiation. Report to the international commission for solar research on actinometric investigations of solar and atmospheric radiation. *Quarterly Journal of the Royal Meteorological Society, 50*(210), 121–126. https://doi.org/10.1002/qj.49705021008.

Arora, V. (2002). Modeling vegetation as a dynamic component in soil-vegetation-atmosphere transfer schemes and hydrological models. *Reviews of Geophysics, 40*(2), 3-1-3-26. https://doi.org/10.1029/2001RG000103.

Bouchet, R. J. (1963). Evapotranspiration réelle et potentielle, signification climatique. *IAHS Publications, 62*, 134–142.

Brutsaert, W., & Parlange, M. B. (1998). Hydrologic cycle explains the evaporation paradox. *Nature, 396*, 30. https://doi.org/10.1038/23845.

Budyko, M. I. (Ed.). (1974). *Climate and life, translated from Russian by D. H. Miller*. New York: Elsevier.

Bureau of Statistics of Jiangxi (2012). *Jiangxi statistical yearbook.* Beijing: China Statistics Press (in Chinese).

Cai, D., Fraedrich, K., Sielmann, F., Guan, Y., Guo, S., Zhang, L., et al. (2014). Climate and vegetation: An ERA-Interim and GIMMS NDVI analysis. *Journal of Climate, 27*(13), 5111–5118. https://doi.org/10.1175/JCLI-D-13-00674.1.

Carmona, A. M., Poveda, G., Sivapalan, M., Vallejo-Bernal, S. M., & Bustamante, E. (2016). A scaling approach to Budyko's framework and the complementary relationship of evapotranspiration in humid environments: Case study of the Amazon River basin. *Hydrology and Earth System Sciences, 20*, 589–603. https://doi.org/10.5194/hess-20-589-2016.

Chattopadhyay, N., & Hulme, M. (1997). Evaporation and potential evapotranspiration in India under conditions of recent and future climate change. *Agricultural and Forest Meteorology, 87*(1), 55–73. https://doi.org/10.1016/S0168-1923(97)00006-3.

Chen, D., Gao, G., Xu, C., Guo, J., & Ren, G. (2005). Comparison of the Thornthwaite method and pan data with the standard Penman-Monteith estimates of reference evapotranspiration in China. *Climate Research, 28*(2), 123–132. https://doi.org/10.3354/cr028123.

Chu, R., Li, M., Shen, S., Islam, A. R. M. T., Cao, W., Tao, S., et al. (2017). Changes in reference evapotranspiration and its contributing factors in Jiangsu, a major economic and agricultural province of eastern China. *Water, 9*(7), 486. https://doi.org/10.3390/w9070486.

Cohen, S., Ianetz, A., & Stanhill, G. (2002). Evaporative climate changes at Bet Dagan, Israel, 1964–1998. *Agricultural and Forest Meteorology, 111*(2), 83–91. https://doi.org/10.1016/S0168-1923(02)00016-3.

Computer Network Information Center (2009). *Chinese academy of sciences. 30 m resolution GDEM data. DEM data. Geospatial data cloud site*. (in Chinese) http://www.gscloud.cn/.

Croitoru, A., Piticar, A., Dragotă, C. S., & Burada, D. C. (2013). Recent changes in reference evapotranspiration in Romania. *Global and Planetary Change, 111*, 127–136. https://doi.org/10.1016/j.gloplacha.2013.09.004.

DeBruin, H. A. R. (2009). Time to think: Reflections of a pre-pensioned scintillometer researcher. *Bulletin of the American Meteorological Society, 90*(5), ES17–ES26. https://doi.org/10.1175/2008BAMS2704.2.

Donohue, R. J., McVicar, T. R., & Roderick, M. L. (2010). Assessing the ability of potential evaporation formulations to capture the dynamics in evaporative demand within a changing climate. *Journal of Hydrology, 386*(1-4), 186–197. http://10.1016/j.jhydrol.2010.03.020.

Fu, B. (1981). On the calculation of the evaporation from land surface. *Chinese Journal of Atmospheric Sciences, 5*(1), 23–31 (in Chinese).

Fu, G., Liu, C., Chen, S., & Hong, J. (2004). Investigating the conversion coefficients for free water surface evaporation of different evaporation pans. *Hydrological Processes, 18*(12), 2247–2262. https://doi.org/10.1002/hyp.5526.

Fu, G., Charles, S. P., & Yu, J. (2009). A critical overview of pan evaporation trends over the last 50 years. *Climatic Change, 97*(1), 193–214. https://doi.org/10.1007/s10584-009-9579-1.

Gao, P., Mu, X., Wang, F., & Li, R. (2011). Changes in streamflow and sediment discharge and the response to human activities in the middle reaches of the Yellow River. *Hydrology and Earth System Sciences Discussions, 7*, 6793–6822. https://doi.org/10.5194/hessd-7-6793-2010.

Giridharan, R., & Emmanuel, R. (2018). The impact of urban compactness, comfort strategies and energy consumption on tropical urban heat island intensity: A review. *Sustainable Cities and Society, 40*, 677–687. https://doi.org/10.1016/j.scs.2018.01.024.

Gober, P., Sampson, D. A., Quay, R., White, D. D., & Chow, W. T. L. (2016). Urban adaptation to mega-drought: Anticipatory water modeling, policy, and planning for the urban Southwest. *Sustainable Cities and Society, 27*, 497–504. https://doi.org/10.1016/j.scs.2016.05.001.

Golubev, V. S., Lawrimore, J. H., Groisman, P. Y., Speranskaya, N. A., Zhuravin, S. A., Menne, M. J., et al. (2001). Evaporation changes over the contiguous United States and the former USSR: A reassessment. *Geophysical Research Letters, 28*(13), 2665–2668. https://doi.org/10.1029/2000GL012851.

Gosset, W. S. (1942). In E. S. Pearson, & J. Wishart (Eds.). *" Student's" collected papers.* Cambridge: Cambridge university press.

Guo, H., Hu, Q., & Jiang, T. (2008). Annual and seasonal streamflow responses to climate and land-cover changes in the Poyang Lake basin. *China. Journal of Hydrology, 355*(1-4), 106–122. https://doi.org/10.1016/j.jhydrol.2008.03.020.

Hardin, E., AghaKouchak, A., Qomi, M. J. A., Madani, K., Tarroja, B., Zhou, Y., et al. (2017). California drought increases CO_2 footprint of energy. *Sustainable Cities and Society, 28*, 450–452. https://doi.org/10.1016/j.scs.2016.09.004.

Hember, R. A., Coops, N. C., & Spittlehouse, D. L. (2017). Spatial and temporal variability of potential evaporation across North American forests. *Hydrology, 4*, 5. https://doi.org/10.3390/hydrology4010005.

Hobbins, M. T., Dai, A., Roderick, M. L., & Farquhar, G. D. (2008). Revisiting the parameterization of potential evaporation as a driver of long-term water balance trends. *Geophysical Research Letters, 35*, L12403. https://doi.org/10.1029/2008GL033840.

Hong, J., Zhong, X., Guo, S., Liu, G., Shen, G. Q., & Yu, T. (2019). Water-energy nexus and its efficiency in China's construction industry: Evidence from province-level data. *Sustainable Cities and Society, 48*, 101557. https://doi.org/10.1016/j.scs.2019.101557.

Lawrimore, J. H., & Peterson, T. C. (2000). Pan evaporation trends in dry and humid regions of the United States. *Journal of Hydrometeorology, 1*, 543–546. https://doi.org/10.1175/1525-7541(2000)001<0543:PETIDA>2.0.CO;2.

Liu, B., Xu, M., Henderson, M., & Gong, W. (2004). A spatial analysis of pan evaporation trend in China, 1955-2000. *Journal of Geophysical Research Atmospheres, 109*, D15102. https://doi.org/10.1029/2004JD004511.

McVicar, T. R., Roderick, M. L., Donohue, R. J., Li, L. T., Niel, T. G. V., Thomas, A., et al. (2012). Global review and synthesis of trends in observed terrestrial near-surface wind speeds: Implications for evaporation. *Journal of Hydrology, 416-417*, 182–205. https://doi.org/10.1016/j.jhydrol.2011.10.024.

McVicar, T. R., Roderick, M. L., Donohue, R. J., & Niel, T. G. V. (2012). Less bluster ahead? Ecohydrological implications of global trends of terrestrial near-surface wind speeds. *Ecohydrology, 5*(4), 381–388 http://doi.org/10.1002/eco.1298.

Milly, P. C. D. (1994). Climate, soil water storage, and the average annual water balance. *Water Resources Research, 30*(7), 2143–2156. https://doi.org/10.1029/94WR00586.

Milly, P. C. D., & Dunne, K. A. (2016). Potential evapotranspiration and continental drying. *Nature Climate Change, 6*, 946–949. https://doi.org/10.1038/NCLIMATE3046.

Moene, A. F., Beyrich, F., & Hartogensis, O. K. (2009). Developments in scintillometry. *Bulletin of the American Meteorological Society, 90*(5), 694–698. https://doi.org/10.1175/2008BAMS2672.1.

Moonen, A. C., Ercoli, L., Mariotti, M., & Masoni, A. (2002). Climate change in Italy indicated by agromete-orological indices over 122 years. *Agricultural and Forest Meteorology, 111*(1), 13–27. https://doi.org/10.1016/S0168-1923(02)00012-6.

Nachshon, U., Netzer, L., & Livshitz, Y. (2016). Land cover properties and rain water harvesting in urban environments. *Sustainable Cities and Society, 27*, 398–406. https://doi.org/10.1016/j.scs.2016.08.008.

Nakamichi, T., & Moroizumi, T. (2015). Applicability of three complementary relationship models for estimating actual evapotranspiration in urban area. *Journal of Hydrology and Hydromechanics, 63*(2), 117–123. https://doi.org/10.1515/johh-2015-0011.

Nash, J. E., & Sutcliffe, J. V. (1970). River flow forecasting through conceptual models part I-A discussion of principles. *Journal of Hydrology, 10*, 282–290. https://doi.org/10.1016/0022-1694(70)90255-6.

National Meteorological Information Center (2019). *Dataset of daily climate data from Chinese surface stations. Surface data and products, v3.0.* (in Chinese) http://data.cma.cn/site/index.html.

Ning, T., Li, Z., Liu, W., & Han, X. (2016). Evolution of potential evapotranspiration in the northern Loess Plateau of China: recent trends and climatic drivers. *International Journal of Climatology, 36*(12), 4019–4028. https://doi.org/10.1002/joc.4611.

Ozturk, M. (2015). An evaluation of global solar radiation empirical formulations in Isparta. *Turkey. Energy Sources, 37*(22), 2474–2486. https://doi.org/10.1080/15567036.2012.745037.

Papaioannou, G., Kitsara, G., & Athanasatos, S. (2011). Impact of global dimming and brightening on reference evapotranspiration in Greece. *Journal of Geophysical Research, 116*, D09107. https://doi.org/10.1029/2010JD015525.

Penman, H. L. (1948). Natural evaporation from open water, bare soil and grass. *Proceedings of the Royal Society of London Series A, Mathematical and Physical Sciences, 193*(1032), 120–145.

Peterson, T. C., Golubev, V. S., & Groisman, P. Y. (1995). Evaporation losing its strength. *Nature, 377*, 687–688. https://doi.org/10.1038/377687b0.

Pettitt, A. N. (1979). A non-parametric approach to the change-point problem. *Journal of the Royal Statistical Society Series C, Applied Statistics, 28*(2), 126–135. http://10.2307/2346729.

Pinzon, J. E., & Tucker, C. J. (2016). *GIMMS NDVI3g Data. Ecocast data, v1.* https://ecocast.arc.nasa.gov/data/pub/gimms/3g.v1/.

Pinzon, J. E., & Tucker, C. J. (2014). A non-stationary 1981–2012 AVHRR NDVI3g time series. *Remote Sensing, 6*(8), 6929–6960. https://doi.org/10.3390/rs6086929.

Remondi, F., Burlando, P., & Vollmer, D. (2016). Exploring the hydrological impact of increasing urbanisation on a tropical river catchment of the metropolitan Jakarta. *Indonesia. Sustainable Cities and Society, 20*, 210–221. https://doi.org/10.1016/j.scs.

2015.10.001.
Roads, J. (2003). The NCEP-NCAR, NCEP-DOE, and TRMM tropical atmosphere hydrologic cycles. *Journal of Hydrometeorology, 4*(5), 826–840. https://doi.org/10.1175/1525-7541(2003)004<0826:TNNATT>2.0.CO;2.
Roberge, F., & Sushama, L. (2018). Urban heat island in current and future climates for the island of Montreal. *Sustainable Cities and Society, 40*, 501–512. https://doi.org/10.1016/j.scs.2018.04.033.
Roderick, M. L., & Farquhar, G. D. (2002). The cause of decreased pan evaporation over the past 50 years. *Science, 298*(5597), 1410–1411. http://10.1126/science.1075390-a.
Roderick, M. L., & Farquhar, G. D. (2004). Changes in Australian pan evaporation from 1970 to 2002. *International Journal of Climatology, 24*(9), 1077–1090. https://doi.org/10.1002/joc.1061.
Roderick, M. L., & Farquhar, G. D. (2005). Changes in New Zealand pan evaporation since the 1970s. *International Journal of Climatology, 25*(15), 2031–2039. https://doi.org/10.1002/joc.1262.
Roderick, M. L., Rotstayn, L. D., Farquhar, G. D., & Hobbins, M. T. (2007). On the attribution of changing pan evaporation. *Geophysical Research Letters, 34*(17), L17403 http://doi.org/1029/2007GL031166.
Sarangi, A., Madramootoo, C. A., & Enright, P. (2006). Comparison of spatial variability techniques for runoff estimation from a Canadian watershed. *Biosystems Engineering, 95*(2), 295–308. https://doi.org/10.1016/j.biosystemseng.2006.06.002.
Shen, Y., Liu, C., Liu, M., Zeng, Y., & Tian, C. (2010). Change in pan evaporation over the past 50 years in the arid region of China. *Hydrological Processes, 24*(2), 225–231. https://doi.org/10.1002/hyp.7435.
Shuttleworth, W. J. (1993). *Evaporation in handbook of hydrology.* Sydney: McGraw-Hill.
Solignac, P. A., Brut, A., Selves, J. L., Béteille, J. P., Gastellu-Etchegorry, J. P., Keravec, P., et al. (2009). Uncertainty analysis of computational methods for deriving sensible heat flux values from scintillometer measurements. *Atmospheric Measurement Techniques, 2*, 1383–1417. https://doi.org/10.5194/amt-2-741-2009.
Stanhill, G., & Möller, M. (2008). Evaporative climate change in the British Isles. *International Journal of Climatology, 28*(9), 1127–1137. https://doi.org/10.1002/joc.1619.
Sun, F. (2007). *Study on watershed evapotranspiration based on the Budyko Hypothesis.* Beijing: Tsinghua University 114 pp. (In Chinese with English abstract).
Thomas, A. (2000). Spatial and temporal characteristics of potential evapotranspiration trends over China. *International Journal of Climatology, 20*(4), 381–396. https://doi.org/10.1002/(SICI)1097-0088(20000330)20:4<381::AID-JOC477>3.0.CO;2-K.
Tsai, W. (2017). Implementation status of Taiwan carbon footprint (CFP) system and a case study of the Taiwan High Speed Rail Corporation. *Sustainable Cities and Society, 35*, 331–335. https://doi.org/10.1016/j.scs.2017.08.021.
Ukkola, A. M., & Prentice, I. C. (2013). A worldwide analysis of trends in water-balance evapotranspiration. *Hydrology and Earth System Sciences, 17*(10), 4177–4187. https://doi.org/10.5194/hess-17-4177-2013.
Vallis, G. K., Zurita-Gotor, P., Cairns, C., & Kidston, J. (2015). Response of the large-scale structure of the atmosphere to global warming. *Quarterly Journal of the Royal Meteorological Society, 141*(690), 1479–1501. https://doi.org/10.1002/qj.2456.
Wang, K., & Dickinson, R. E. (2012). A review of global terrestrial evapotranspiration: Observation, modeling, climatology, and climatic variability. *Reviews of Geophysics, 50*(2), RG2005. https://doi.org/10.1029/2011RG000373.
Wang, D., & Hejazi, M. (2011). Quantifying the relative contribution of the climate and direct human impacts on mean annual streamflow in the contiguous United States. *Water Resources Research, 47*, W00J12. https://doi.org/10.1029/2010WR010283.
Wang, Y., Feng, Y., Zuo, J., & Rameezdeen, R. (2019). From "Traditional" to "Low carbon" urban land use: Evaluation and obstacle analysis. *Sustainable Cities and Society, 51*, 101722. https://doi.org/10.1016/j.scs.2019.101722.
Wang, Y., Liu, B., Zhai, J., Su, B., Luo, Y., & Zhang, Z. (2011). Relationship between potential and actual evaporation in Yangtze River basin. *Advances in Climate Change Research, 7*(6), 393–399 (In Chinese with English abstract).
Wang, Z., Xie, P., Lai, C., Chen, X., Wu, X., Zeng, Z., et al. (2017). Spatiotemporal variability of reference evapotranspiration and contributing climatic factors in China during 1961–2013. *Journal of Hydrology, 544*, 97–108. https://doi.org/10.1016/j.jhydrol.2016.11.021.
Wild, M., Ohmura, A., Gilgen, H., & Rosenfeld, D. (2004). On the consistency of trends in radiation and temperature records and implications for the global hydrological cycle. *Geophysical Research Letters, 31*, L11201. https://doi.org/10.1029/2003GL019188.
Wolock, D. M., & McCabe, G. J. (1999). Explaining spatial variability in mean annual runoff in the conterminous United States. *Climate Research, 11*, 149–159. https://doi.org/10.3354/cr011149.
World Meteorological Organization (WMO) (2014). *Measurement of evaporation, in WMO guide to meteorological instruments and methods of observation*Switzerland: Geneva, (Chapter 10). Available at(8th ed.). https://library.wmo.int/opac/doc_num.php?explnum_id=3156.
Xu, Y., Pan, S., Gao, C., Fu, G., & Chiang, Y. (2016). Historical pan evaporation changes in the Qiantang River Basin, East China. *International Journal of Climatology, 36*, 1928–1942. https://doi.org/10.1002/joc.4470.
Yan, D., Schneider, U. A., Schmid, E., Huang, H. Q., Pan, L., & Dilly, O. (2013). Interactions between land use change, regional development, and climate change in the Poyang Lake district from 1985 to 2035. *Agricultural Systems, 119*, 10–21. https://doi.org/10.1016/j.agsy.2013.04.001.
Yang, H., & Yang, D. (2012). Climatic factors influencing changing pan evaporation across China from 1961 to 2001. *Journal of Hydrology, 414-415*, 184–193. https://doi.org/10.1016/j.jhydrol.2011.10.043.
Yang, D., Sun, F., Liu, Z., Cong, Z., & Lei, Z. (2006). Interpreting the complementary relationship in non-humid environments based on the Budyko and Penman hypotheses. *Geophysical Research Letters, 33*(18), L18402. https://doi.org/10.1029/2006GL027657.
Yang, D., Sun, F., Liu, Z., Cong, Z., Ni, G., & Lei, Z. (2007). Analyzing spatial and temporal variability of annual water-energy balance in nonhumid regions of China using the Budyko hypothesis. *Water Resources Research, 43*, W04426. https://doi.org/10.1029/2006WR005224.
Ye, X., Zhang, Q., Bai, L., & Hu, Q. (2011). A modeling study of catchment discharge to Poyang Lake under future climate in China. *Quaternary International, 244*(2), 221–229. https://doi.org/10.1016/j.quaint.2010.07.004.
Zhang, L., Traore, S., Cui, Y., Luo, Y., Zhu, G., Liu, B., et al. (2019). Assessment of spatiotemporal variability of reference evapotranspiration and controlling climate factors over decades in China using geospatial techniques. *Agricultural Water Management, 213*(C), 499–511. https://doi.org/10.1016/j.agwat.2018.09.037.
Zhang, Q., Liu, C., Xu, C., Xu, Y., & Jiang, T. (2006). Observed trends of annual maximum water level and streamflow during past 130 years in the Yangtze River basin. *China. Journal of Hydrology, 324*(1-4), 255–265. https://doi.org/10.1016/j.jhydrol.2005.09.023.
Zhang, Y., Leuning, R., Chiew, F. H. S., Wang, E., Zhang, L., Liu, C., et al. (2012). Decadal trends in evaporation from global energy and water balances. *Journal of Hydrometeorology, 13*(1), 379–391. https://doi.org/10.1175/JHM-D-11-012.1.
Zuo, H., Chen, B., Wang, S., Guo, Y., Zuo, B., Wu, L., et al. (2016). Observational study on complementary relationship between pan evaporation and actual evapotranspiration and its variation with pan type. *Agricultural and Forest Meteorology, 222*, 1–9. https://doi.org/10.1016/j.agrformet.2016.03.002.